frontiers | Frontiers in Astronomy and Space Sciences

ORIGINAL RESEARCH
published: 29 April 2022
doi: 10.3389/fspas.2022.866023

Effect of Solar Wind Pressure and Substorm Linked Particle Injection on Local Time Distribution of Electromagnetic Ion Cyclotron Waves

Aditi Upadhyay , Bharati Kakad , Amar Kakad and R. Rawat*

Indian Institute of Geomagnetism, New Panvel, India

Several observations of electromagnetic ion cyclotron (EMIC) waves have been reported from the Earth's magnetosphere. It is an important component of space weather research due to its efficient role in precipitating highly energetic electrons from the Earth's radiation belt. In general, the interplanetary solar wind conditions and geomagnetic activity control the generation of EMIC waves by modifying the ambient plasma conditions in the generation region. Therefore, EMIC wave occurrence patterns observed both in space and on the ground are influenced by the variations in the parameters like auroral electrojet (*AE* index), solar wind dynamic pressure, and *Dst*, which represent the magnetospheric conditions. We present a detailed local time distribution of EMIC waves observed at the Antarctic station, Maitri (geographic 70.7^{o}S, 11.8^{o}E, L = 5), for 2011–2017. We have cataloged the EMIC wave occurrence in four frequency ranges (between 0.12–2 Hz) and examined their occurrence pattern for different levels of *AE* index and solar wind pressure. The present analysis reveals that at the ground station, Maitri, the occurrence of EMIC waves is dominated in the lower frequency range (0.12–1 Hz) with lower occurrence in the higher frequency range (>1Hz). It is found that the EMIC waves having frequencies > 1 Hz occur dominantly in the early morning hours with a peak close to 5.7 LT hours, and they are linked to the magnetic activity that occurred in the preceding days, whereas the effect of solar wind dynamic pressure and *AE* index on the local time occurrence of EMIC waves is unambiguously seen for the waves with <1 Hz. The study revealed the larger *AE* index shifts occurrence of EMIC waves in the dusk sector.

Keywords: EMIC wave, geomagnetic activity, substorm, inner magnetosphere, Pc1-Pc2 pulsations

OPEN ACCESS

Edited by:
Ankush Bhaskar,
Vikram Sarabhai Space Centre, India

Reviewed by:
Huishan Fu,
Beihang University, China
Peter Haesung Yoon,
University of Maryland, College Park, United States

****Correspondence:***
Aditi Upadhyay
aditiu147@gmail.com

Specialty section:
This article was submitted to Space Physics, a section of the journal Frontiers in Astronomy and Space Sciences

Received: *30 January 2022*
Accepted: *28 March 2022*
Published: *29 April 2022*

Citation:
Upadhyay A, Kakad B, Kakad A and Rawat R (2022) Effect of Solar Wind Pressure and Substorm Linked Particle Injection on Local Time Distribution of Electromagnetic Ion Cyclotron Waves. Front. Astron. Space Sci. 9:866023. doi: 10.3389/fspas.2022.866023

1 INTRODUCTION

The electromagnetic ion cyclotron (EMIC) waves fall into the ultralow frequency range (0.1–5 Hz) commonly referred to as Pc1–Pc2 pulsations. The EMIC waves are known for precipitating the relativistic electrons and ring current ions through pitch angle scattering (Thorne and Kennel, 1971; Summers and Thorne, 2003; Sandanger et al., 2007) and are responsible for ion heating (Horne and Thorne, 1997; Yuan et al., 2014) and proton auroras (Sakaguchi et al., 2015; Ozaki et al., 2021). These waves are generated in the equatorial regions over a wide range of L-shell due to the anisotropic distribution of ring current ions (Cornwall, 1965; Anderson et al., 1996). Different aspects of EMIC waves have been examined using both ground and satellite data to

gather more information about their occurrence, characteristics, MLT-azimuthal-radial extent, etc. (Usanova et al., 2008; Posch et al., 2010; Usanova et al., 2013; Mann et al., 2014; Allen et al., 2015; Engebretson et al., 2015; Blum et al., 2017; Yu et al., 2017; Wang et al., 2021). The gyrofrequency of the ion responsible for the generation of the wave determines the frequency band (H^+ or He^+) of these waves. The global distribution of EMIC wave occurrence has been widely explored by several past satellite missions. The DE-1 spacecraft surveyed the inner magnetosphere (3 > L-shell>5) and reported the dusk sector is the preferential zone for the generation of the EMIC waves (Erlandson and Ukhorskiy, 2001). L-shell is a distance of magnetic field line in the magnetic equatorial plane in units of Earth radii. By using AMPTE satellite data, Anderson et al. (1992) have shown that the EMIC waves are primarily observed at $L > 7$ in the afternoon sector, which is consistent with the recent results by Keika et al. (2013) and GOES spacecraft observations (Clausen et al., 2011). The CRESS spacecraft gave broader time coverage, and these observations indicated that 80% of the EMIC waves occur during 13–20 magnetic local time for $L > 3$ (Meredith et al., 2003). A recent study by Min et al. (2012) has used THEMIS spacecraft data and reported two peaks in the EMIC wave occurrence probability: one in the dawn sector (dominated by *H* band waves) and the other in the dusk (dominated by *He* band waves). All these scenarios are based on satellite observations.

After the generation, the EMIC waves propagate along geomagnetic field lines from their source in the equatorial region to the mid- and high-latitude ionosphere. A part of EMIC wave energy can get trapped in the F-region ionospheric duct and propagate horizontally to lower or higher latitudes. Thus, EMIC wave signatures can be observed on the ground as well. However, due to ducted propagation, we do not have any information about L-shell associated with their source locations. Unlike satellite observations, it is difficult to associate the EMIC wave signatures observed on the ground to a particular band (H^+ or He^+) due to its propagation through ionospheric ducts. However, the EMIC wave event observed on the ground is the manifestation of the EMIC wave generation in the magnetosphere at a particular L-shell. Thus, the ground EMIC wave observations are also widely used to examine the characteristics of these waves. The diurnal distribution has been studied using the ground-based EMIC wave observations from Sodankylāics geophysical observatory (L = 5.2) for the maxima and minima of the 21st solar cycle (Mursula et al., 1991, 1996). These authors also observed two peak structures in the occurrence pattern, but the morning peak was shown by structured and the afternoon–dusk peak by unstructured pulsations. A similar study from an observatory (Davis station, geomagnetic 74.7^oS 100.8^oE) located in the polar cusp showed a single peak around local noon in the occurrence of the EMIC waves (Morris and Cole, 1991). A recent study by Upadhyay et al. (2020) indicated that the occurrence of EMIC wave peaks around the afternoon–dusk sector. In all the above ground-based studies, not much attention was given to the frequencies of the EMIC waves. Particularly, the local time distribution of EMIC waves in different frequency ranges has not been explored well with the ground observations.

The EMIC waves are typically generated by the temperature anisotropy ($T_\perp > T_\parallel$) of medium energy (1–100 keV) ring current protons (Kennel and Petschek, 1966). There can be multiple reasons for the enhancement in the anisotropy of the ions; one of the recognized sources is the energetic particle injections into the inner magnetosphere during storms and substorms (Liu et al., 2019). The geomagnetic storms and substorms enhance the earthward convection of ring current ions in the inner magnetosphere, which leads to an increase in the anisotropic distribution of ions and eventually assist in the excitation of the EMIC waves (Criswell, 1969). Another possible source is the solar wind pressure. The compression of the magnetopause due to an increase in solar wind pressure leads to an increase in the anisotropy of the ions by the process of betatron acceleration (McCollough et al., 2010; Fu et al., 2012a,b; Park et al., 2016; Xue et al., 2021). As multiple factors control the generation of EMIC waves, many statistical studies have been conducted using satellite data to understand the role of different interplanetary parameters and magnetospheric conditions in the generation of the EMIC waves. For example, solar wind dynamic pressure pulses contribute positively to the growth of EMIC waves observed on the dayside (Usanova et al., 2012; Remya et al., 2015; Liu et al., 2019). The association of solar wind pressure and EMIC wave generation is reflected in the ground observations as well. A survey of ground EMIC waves has revealed that most of the EMIC wave events were linked with an increase in the solar wind dynamic pressure (Regi et al., 2017). On the contrary, the ion injections from the magnetotail, enhanced convection, and substorms are known to trigger the generation of EMIC waves observed in the dusk side (Jordanova et al., 2001; Kim et al., 2017; Remya et al., 2018). The auroral electrojet (*AE*) index is one of the proxies, which is used to identify the substorm (Davis and Sugiura, 1966). Meredith et al. (2014) studied the effect of the *AE* index on the occurrence of *H* and *He* band EMIC waves. Keika et al. (2013) have studied the global occurrence of EMIC waves using satellite data and attributed their excitation to two independent processes: 1) externally triggered waves on the dayside that are driven by solar wind pressure and 2) the internally excited waves in the dusk side caused by the energetic ion injections from the midnight sector. In addition, these authors reported that during the quiet time, the occurrence of EMIC waves is more likely in the morning sector. Above all studies hint that overall, the EMIC wave generation is likely in the afternoon, evening, and morning sectors, which are associated with different triggering source mechanisms. Thus, a detailed investigation of the local time distribution of EMIC waves in different frequency ranges to understand underlined physical processes is worthwhile.

In this context, we present the local time distribution of EMIC waves in different frequency ranges and their dependence on the solar wind pressure and auroral electrojet indices using long-term ground observations from the Indian Antarctic station, Maitri. The article is organized as follows: The information about the experimental setup and identification of the EMIC waves are detailed in **Section 2**. The results are presented in **Section 3** and discussed in **Section 4**. The present work is summarized and concluded in **Section 5**.

2 DATA USED AND EMIC WAVE IDENTIFICATION

In the present study, we have utilized ground induction coil magnetometer (ICM) data recorded at the Indian Antarctic station, Maitri (geographic lat. 70.7^o S, geographic long. 11.8^o E, L≈5) for the period of 2011–2017. The ICM consists of three magnetic coil sensors, which record the magnetic field fluctuations in N-S, E-W, and vertical directions. The data are sampled at either 64 Hz or 256 Hz. For each day, the variations in three components of the magnetic field, namely, B_x, B_y, and B_z are used to get the Fourier spectrogram. The power spectral density in the spectrogram of total magnetic field variation is obtained from $B(f,t) = P_x(f,t) + P_y(f,t) + P_z(f,t)$. Here, $P_x(f,t)$, $P_y(f,t)$, and $P_z(f,t)$ are the power spectral densities of individual magnetic field components B_x, B_y, and B_z, respectively. The spectrogram represents the magnetic field power $B(f,t)$ in the frequency–time domain with the resolution of 0.011 Hz and 18 s, and it is in the units of nT^2/Hz. We noticed that at Maitri, the observed EMIC wave frequencies predominantly lie below 2 Hz and occasionally exceed 2 Hz. Therefore, EMIC wave occurrence is noted in four frequency bins as 1) f_1 = 0.12–0.5 Hz, 2) f_2 = 0.5–1 Hz, 3) f_3 = 1–1.5 Hz, and 4) f_4 = 1.5– 2 Hz. These frequency limits are not associated with the EMIC wavebands; it is simply to separate EMIC waves into four categories based on the frequencies associated with the EMIC wave observed at ground station Maitri. For each day, we checked the average power in the spectrogram (i.e., $\langle B(f,t)\rangle$) corresponding to each frequency range. Using the Fourier spectrogram, one can identify the presence/absence of the wave in the Pc1–Pc2 range, and time variations of average power, $\langle B(f,t)\rangle$ in different frequency ranges allow us to verify whether or not the EMIC wave power is above the noise level. This way, we identified the presence/absence of EMIC waves and cataloged their details like frequency range and start and end time. In our study, we have also used hourly values of solar wind dynamic pressure, and geomagnetic activity indices like *AE*, *Dst*, and *Kp* from OMNIWeb. We would like to highlight the fact that, unlike the satellite observations, the frequency bins used here do not give any direct information about the source ions and generation region of EMIC waves. This is due to the

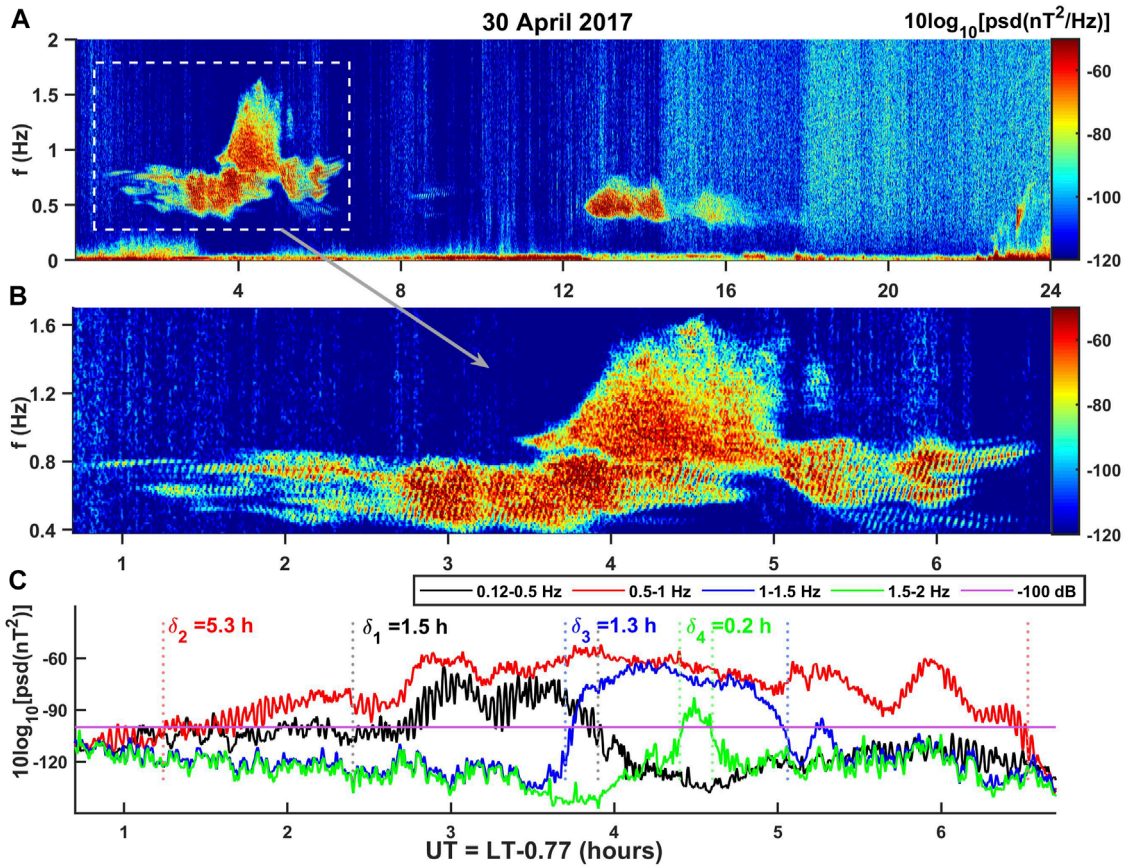

FIGURE 1 | (A) Spectrogram of total magnetic field variation on 30 April 2017. The presence of EMIC waves is clearly evident. The power is expressed in dB (i.e., 10 log[psd]). The dotted box marks one EMIC wave event that occurred between 0.6 and 6.6 UT hours, and its enlarged view is depicted in **(B)**. **(C)** Time variation of average spectrogram power for different frequency ranges, namely, f_1, f_2, f_3, and f_4. Here, UT = LT-0.77 h. The intervals of EMIC wave activities are marked with vertical dotted lines. δ_{1-4}, respectively, represents the duration of the EMIC wave in different frequency ranges.

TABLE 1 | Duration of EMIC wave occurrence in different frequency ranges as observed at the ground station, Maitri (geographic 70.7^{O}S, 11.8^{O}E, L = 5), for quiet days of 2011–2017.

Frequency range (Hz)	Duration (hours)	Percentage (%)
f_1 = 0.12–0.5	1968.9	61.7
f_2 = 0.5–1	1082.8	33.9
f_3 = 1–1.5	124.8	3.9
f_4 = 1.5–2	16.9	0.5

fact that the propagation of EMIC waves along magnetic field lines and their ducting through the ionosphere attenuate wave frequency and amplitude (Johnson and Cheng, 1999; Kim and Johnson, 2016). All ICM data on magnetically quiet days are considered in the present study. A day is considered magnetically quiet if the *Ap* value for that day or the previous day is less than 20.

As an illustration, we have shown one example of EMIC waves that occurred on 30 April 2017 in **Figure 1**. **Figure 1A** shows the Fourier spectrogram of variation in total magnetic field recorded by ICM for the entire day, wherein two distinct EMIC wave events are clearly visible. We have highlighted one EMIC wave event with a dotted rectangle, which has an extended frequency range. In **Figure 1B**, we have shown an enlarged view of the highlighted event. For this highlighted event, **Figure 1C** shows the variation of the average power of the Fourier spectrogram (i.e., $\langle B(f,t)\rangle$) for four different frequency ranges f_1 (black), f_2 (red), f_3 (blue), and f_4 (green). The horizontal line at -100 dB represents the cutoff used to select the EMIC wave events with significant power. We have observed that in the Fourier spectrogram, the average power generally falls below -100 dB in the absence of EMIC wave activity. Therefore, we chose this limit. The horizontal dotted line indicates the EMIC wave power above -100 dB (i.e., >10^{-5}nT/Hz) in respective frequency ranges, and their durations are 2.4–3.97, 1.2–6.5, 3.7–5.0, and 4.4–4.6 UT hours for f_1, f_2, f_3, and f_4 frequency ranges, respectively. Here, UT = LT-0.77 h. This way, we have cataloged all EMIC wave events, and the total occurrence of EMIC waves in different frequency ranges is summarized in **Table 1**. It is found that the EMIC wave occurrence is maximum in the f_1 frequency range, which gradually decreases for f_2 and f_3 frequencies, and it is minimum in the f_4 frequency range. The total occurrence durations of EMIC waves are approximately 1969 h, 1083 h, 125 h, and 17 h for f_1, f_2, f_3, and f_4 frequency ranges, respectively. The percentage of the duration of EMIC wave occurrence in f_1, f_2, f_3, and f_4 frequency ranges are 61.7%, 33.9%, 3.9, and 0.5%, respectively.

3 RESULTS

3.1 Local Time Distribution of Electromagnetic Ion Cyclotron Waves

We have examined the overall occurrence of EMIC waves in different frequency ranges at the ground station, Maitri. In this section, we have studied the local time occurrence patterns of EMIC waves for frequency ranges f_1, f_2, f_3, and f_4. In **Figure 2**, we have plotted the time variation of the probability of occurrence of EMIC waves in different frequency ranges. The time resolution on the x-axis is taken as one hour, and for all EMIC wave occurrences in this one hour, a time-bin is added to get the EMIC occurrence during that hour. These probability distribution functions are normalized by the total EMIC wave duration in the respective frequency ranges. It means that the summation of the probability distribution function over the entire time of 0–24 LT hours is always 100%, which corresponds to the total EMIC wave occurrence in respective frequency ranges. For example, in f_1, f_2, f_3, and f_4 frequency ranges, the 100% corresponds to 1969, 1083, 125, and 17 h, respectively. **Figures 2A,B** indicate that for f_1 and f_2 frequency ranges, the majority of EMIC waves occurred between 12–22 h and 10–18 h, with peak occurrence close to 16 and 14 h, respectively, whereas **Figures 2C,D** depict that for f_3 and f_4 frequency ranges, the EMIC wave occurrence is mainly concentrated in the early morning 2–10 h, with a peak around 6 LT hour. It may be noted that in **Figure 2B** apart from the major peak in EMIC wave occurrence around 14 LT, there is a second peak in occurrence around 5–10 LT. Now the question is how to explain this second peak in the occurrence. Here, the frequency limits chosen to categorize wave events are not stringent rather it is strictly based on the observed EMIC wave frequencies in the ICM data recorded at Maitri. Therefore, some overlap in the trends is expected. However, the likeliness of a shift in peak occurrence of EMIC waves from dusk to dawn sector with an increase in the EMIC wave frequency is clearly evident.

This analysis suggests that there are two favorable local time regimes for the EMIC wave occurrence on the ground; one in the early morning and another is in the afternoon–evening. The frequency characteristics of the EMIC waves observed in these two preferred time sectors are different. The morning time occurrence is mainly associated with the higher frequency (i.e., >1 Hz), whereas the afternoon–evening time occurrence is associated with the lower frequency (<1 Hz) EMIC waves. In order to understand this distinct local time preference for the EMIC wave occurrence, we examined the effect of solar wind pressure and auroral electrojet index (*AE*) on the ground observations of the EMIC waves. Hereafter, we have combined the occurrence in f_3 and f_4 and treated it as a higher frequency as individually the occurrence in f_4 is too low to perform a separate analysis. The results based on solar wind pressure and the *AE* index are discussed in the following subsection.

3.2 Effect of Solar Wind Pressure and *AE* Index

According to previous studies, solar wind dynamic pressure and substorm activity are the potential sources for the generation of EMIC waves (Halford et al., 2010; Usanova et al., 2012; Kim et al., 2017). Increased solar wind dynamic pressure can generate the required temperature anisotropy in the source ion population and it can also change the magnetic field gradient to reduce the threshold wave amplitude needed for the growth of the EMIC wave (Omura et al., 2010). Recently, Remya et al. (2018) have highlighted the role of substorm injected ions in the generation of EMIC waves. The auroral electrojet *AE* index

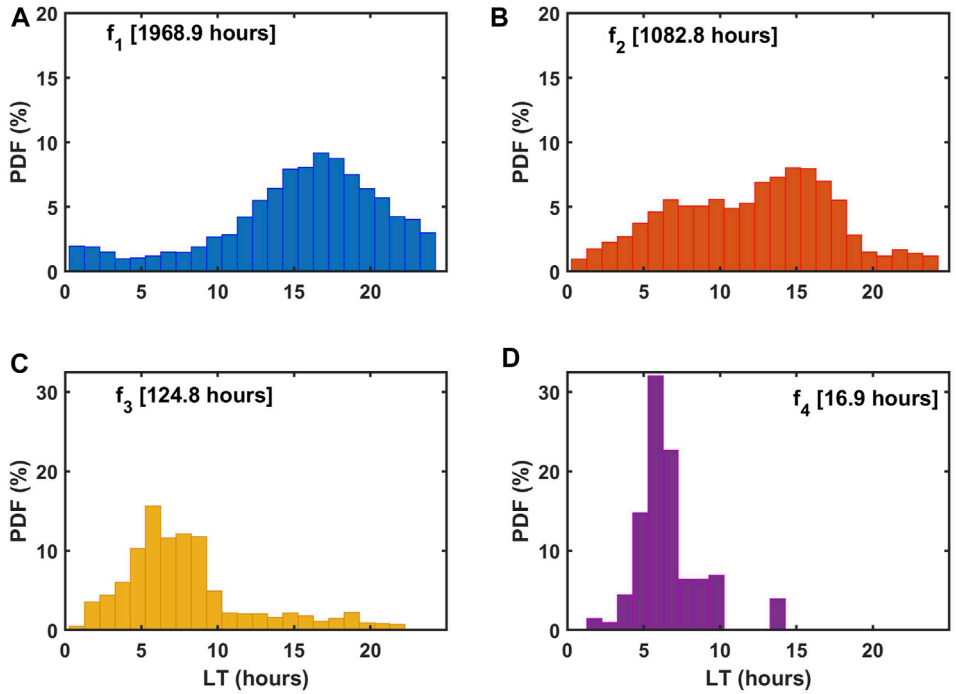

FIGURE 2 | Probability distribution function of EMIC wave occurrence in the four frequency ranges: **(A)** f_1, **(B)** f_2, **(C)** f_3, and **(D)** f_4. The total duration of EMIC wave occurrence under each category is mentioned in respective subplots. The peak for maximum occurrence shifts toward morning hours as the frequency increases from f_1 to f_4.

is commonly used to identify the substorm activity. Thus, to understand whether or not these parameters control the diurnal distribution of EMIC waves on the ground, we have plotted the local time distribution of EMIC wave occurrence for two levels of solar wind pressure and *AE* index. The solar wind pressure and *AE* index during the EMIC wave events are compiled and their probability distribution are shown in **Figures 3A,B**, respectively. We chose a threshold of 2 nPa for solar wind pressure and 150 nT for *AE* index to separate EMIC wave events into two categories. As seen in **Figure 3**, there is a sufficient number of EMIC wave

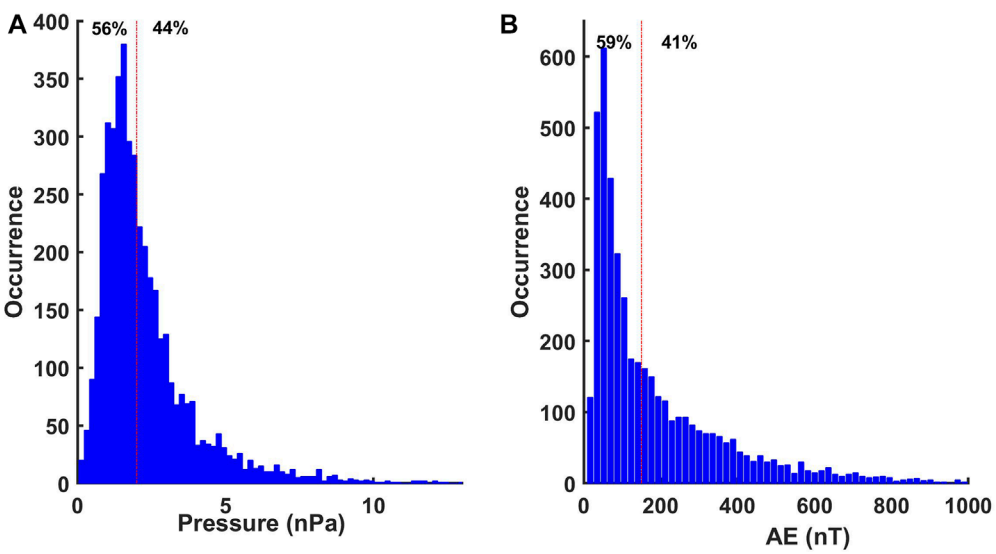

FIGURE 3 | Distribution function of values of **(A)** solar wind pressure and **(B)** *AE* index associated with the EMIC wave occurrence. The level of 2 nPa in the solar wind pressure and 150 nT in the *AE* index is chosen to divide the entire data into two categories. These limits are shown by the red dashed dotted line in respective subplots.

events in both categories of low and high levels of solar wind pressure and *AE* index.

The distribution of EMIC wave occurrence for two levels of solar wind pressure, namely, 1) ≤ 2 nPa (blue color) and 2) > 2 nPa (red color) are shown in left panels of **Figures 4A–C** and corresponds to f_1, f_2, and $f_3 + f_4$ frequency ranges, respectively. Similarly, the distribution of EMIC wave occurrence for two levels of *AE* index: 1) ≤ 150 nT (blue color) and 2) > 150 nT (red color) are shown in **Figures 4D–F**, respectively, for f_1, f_2, and $f_3 + f_4$ frequency ranges. Each probability distribution curve shown in **Figure 4** adds to 100%, and it represents the total EMIC wave occurrence in corresponding categories. These durations are mentioned in the respective subplots of **Figure 4**. For example, as shown in **Figure 4A**, total EMIC wave occurrence in f_1 frequency range for low (≤2 nPa) and high (> 2 nPa) solar wind pressure conditions are 892 and 1061 h, respectively. It may be noted that the sum of these durations is slightly less than the total duration presented in **Figure 2A** because simultaneous solar wind pressure data were not available for a few EMIC wave events. The most evident feature of **Figure 4** is that the high-frequency EMIC wave occurrence in the early morning hours is less significantly affected by the level of solar wind pressure and *AE* index (see panels **Figure 4C,F**). This tendency is discussed in detail in the next subsection, whereas for lower frequency ranges f_1 and f_2, it is noticed that the EMIC wave occurrence shifts toward the dusk sector for higher solar wind pressure and *AE* index, and this tendency is more evident for f_1 than for the f_2 frequency range (see panels **Figures 4A,D** and **Figures 4B,E**).

It is seen that both solar wind pressure and *AE* index affect the diurnal occurrence of EMIC waves. However, we are dealing with two parameters, that is, solar wind pressure and *AE* index. In order to establish the role of either of the parameters individually, one has to verify the EMIC wave occurrence for 1) low and high solar wind pressure by imposing limits on *AE*, and 2) low and high *AE* index by imposing limits on the solar wind pressure. Since the EMIC wave occurrence in higher frequency ranges (>1 Hz) is not significantly affected by the level of solar wind pressure and *AE*, we have performed this investigation for lower frequency ranges only, that is, f_1 and f_2. First, we took all EMIC wave events with *AE* ≤ 150 nT and plotted its probability distribution function for two levels of solar wind pressure: *P* ≤ 2 nPa (blue color) and *P* > 2 nPa (red color) as shown in **Figure 5A**. Next, we considered all EMIC wave events with *AE* > 150 nT and plotted the probability distribution function of EMIC wave occurrence for two levels of solar wind pressure in **Figure 5B**. On similar lines, we segregated EMIC wave events for two levels of solar wind pressure, and then the probability distribution function of EMIC wave occurrence is obtained for *AE* ≤ 150 nT and *AE* > 150 nT, which is shown in **Figures 5C,D**, respectively. The total duration of EMIC waves under each category is mentioned in respective subplots. In **Figure 5B**, it is evident that for higher values of *AE*, the EMIC wave occurrence is localized between 15 and 23 LT

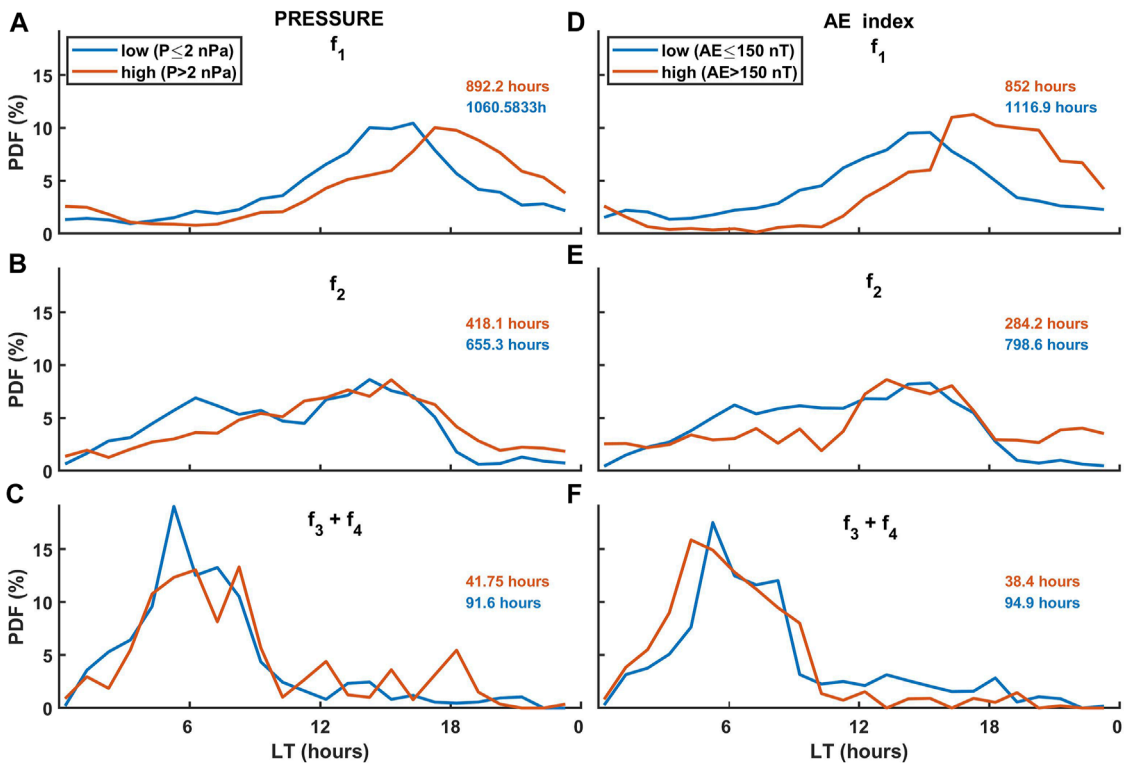

FIGURE 4 | Probability distribution function of EMIC wave occurrence for two levels of solar wind pressure, namely, 1)*P* ≤ 2 nPa (blue color) and 2) *P* > 2 nPa (red color) is shown in **(A–C)** for f_1, f_2, and f_3+f_4 frequency ranges, respectively. The probability distribution of EMIC wave occurrence for two levels of *AE* index, namely, 1) *AE* ≤ 150 nT (blue color) and 2) *AE* > 150 nT (red color) is shown in **(D–F)**, respectively, for f_1, f_2, and $f_3 + f_4$ frequency ranges.

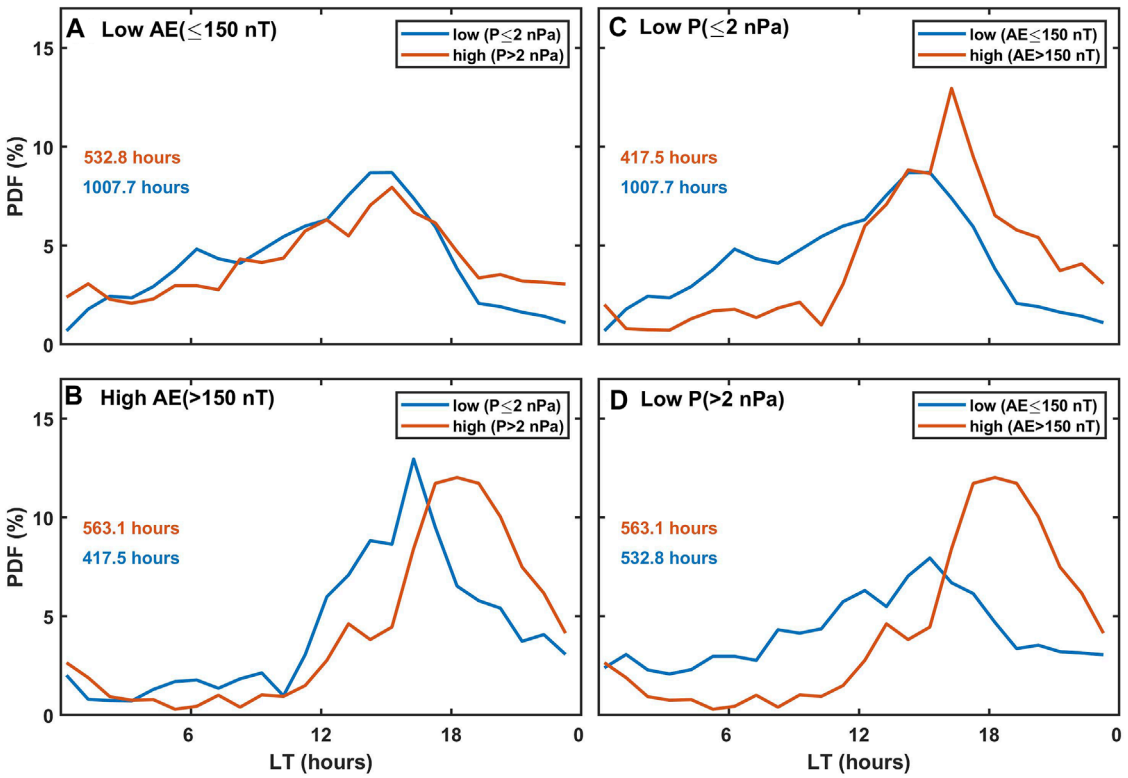

FIGURE 5 | Diurnal distribution of EMIC waves is shown for high and low levels of *AE* by imposing a limit on solar wind pressure, and *vice versa*. The distribution function of EMIC waves for **(A)** $AE \leq 150$ **(B)** $AE > 150$ nT with two levels of solar wind pressure, and the distribution function of EMIC waves for **(C)** $P \leq 2$ nPa and **(D)** $P > 2$ nPa with two levels of *AE* index are plotted. Here, we have considered all EMIC waves associated with the low-frequency range f_1 and f_2.

hours, with a peak close to 17–18 LT hours, and it is irrespective of the level of solar wind pressure. It suggests that when the *AE* index is high, then the EMIC wave occurrence is more probable in the dusk sector, irrespective of high/low solar wind pressure. Similarly, a clear shift toward the evening-midnight sector in the peak occurrence of the EMIC wave is seen for the $AE > 150$ nT as compared to $AE \leq 150$ nT (see **Figures 5C,D**).

Thus, one can say that *AE* plays a significant role in controlling the diurnal distribution of EMIC waves, and it shifts the peak EMIC wave occurrence toward nighttime. Usanova et al. (2012) have reported a similar observation using the THEMIS data. From their observations, it was seen that for low *AE* values, the major contribution came from the noon sector (15–21 MLT), but for higher *AE* values, the contribution from the evening sector (15–21 MLT) is more dominant. It is attributed to the increase in the hot ion population on the night side due to the fresh injection of ions during the increased magnetospheric convection. It has also been proposed that during the high auroral activity, the inner boundary of the ion plasma sheet moves closer to Earth, eventually bringing the drift paths of the injected ions to inner L-shells (Cao et al., 2011). This increases the likelihood of the hot ions passing through the regions of the cold plasma density inside the plasmasphere, thereby making the dusk–midnight sector favorable for the generation of EMIC waves. For the periods of low *AE* index, the EMIC wave occurrence is dominant in the afternoon sector (14–16 LT hours) for both high and low levels of solar wind pressure (see **Figure 5A**). In earlier studies, it is suggested that even with a modest pressure pulse the EMIC waves can be generated (Anderson and Hamilton, 1993; Kakad et al., 2019). This might be the reason for getting nearly similar trends of EMIC wave occurrence for low and high solar wind pressure with its peak localized in the afternoon sector.

3.3 Understanding Early Morning Occurrence of Electromagnetic Ion Cyclotron Waves

In the preceding subsection, we noticed that early morning EMIC wave occurrence in the higher frequency range is unaffected by the level of solar wind pressure and *AE* index. In the past, using ground observations, it was reported that EMIC wave occurrence shifts to the early morning hours in the late recovery phase of the storm, and the associated average frequency of the Pc1 waves is higher than the normal (Bortnik et al., 2008). We verified whether or not a similar tendency is reflected in our statistics of EMIC waves. For this purpose, we carried out epoch analysis and examined the time variation of *Kp* and *Dst* indices for 144 h (6 days) before the start of the EMIC wave event. An illustration for this analysis is shown in **Figure 6**. Spectrogram depicting the presence of EMIC waves in the early morning hours of 1 October

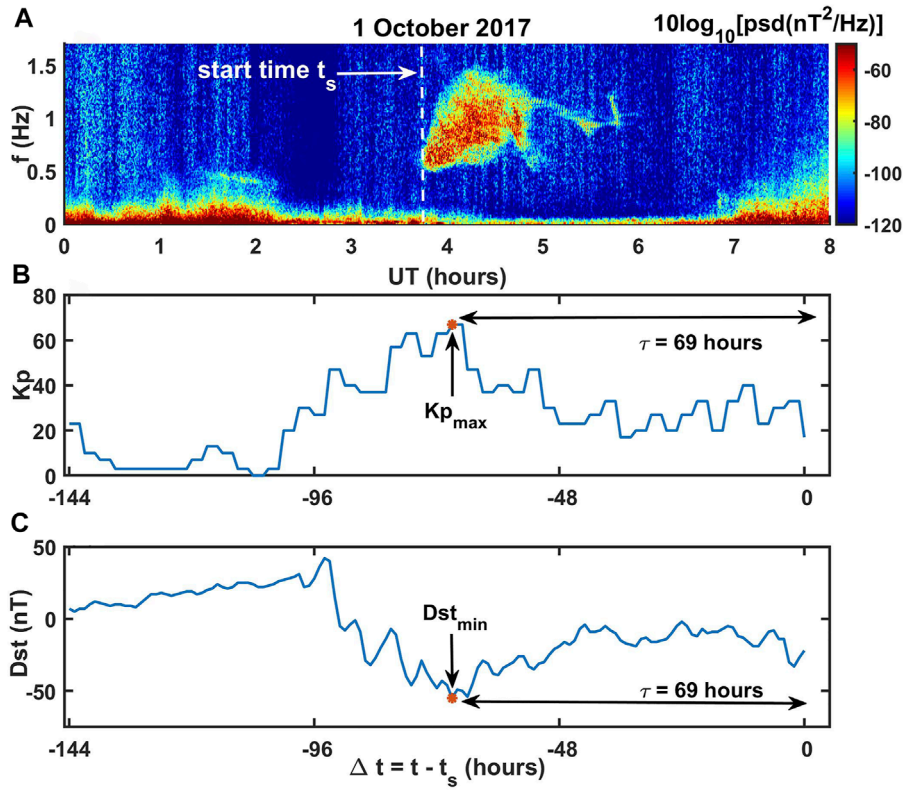

FIGURE 6 | Example of the epoch analysis is illustrated. **(A)** Spectrogram depicts the presence of EMIC waves in the early morning hours of 1 October 2017. The start time of the event is marked as t_s. The variations of **(B)** *Kp* and **(C)** *Dst* for 144 h before the start time t_s are plotted as a function of $\Delta t = t - t_s$. Here, $\Delta t = 0$ indicates the start of the EMIC wave event.

2017 is shown in **Figure 6A**. The start time, t_s, of the EMIC wave event is marked with a vertical dotted line. We shifted the time axis such that $\Delta t = t - t_s$. Here, $\Delta t = 0$ represents the start time of a given EMIC wave event. For 1 October 2017, the variation of *Kp* and *Dst* is plotted as a function of Δt in **Figures 6B,C**, respectively. The maximum in *Kp* and minimum in *Dst* prior to $\Delta t = 0$ are noted and marked with red asterisks in respective subplots. The time lag τ gives the time of maximum *Kp* and minimum *Dst* prior to the occurrence of the EMIC wave. This way we compiled data of Kp_{max} and Dst_{min} for all EMIC wave events associated with f_1, f_2, and $f_3 + f_4$ frequency ranges.

In **Figures 7A,B** the average values of *Kp* and *Dst* index as a function of Δt are plotted, respectively, for f_1, f_2, and $f_3 + f_4$ frequency ranges. For each EMIC wave event, we have corresponding value of Kp_{max} and Dst_{min}. **Figures 7C,D** show the plots of the probability distribution function of Kp_{max} and Dst_{min}, respectively, for f_1, f_2, and $f_3 + f_4$ frequency ranges. This epoch analysis indicates that average *Kp* is considerably higher for higher frequency range $f_3 + f_4$ than that of f_1 and f_2. Similarly, the average *Dst* is lower for higher frequency range $f_3 + f_4$ than that of f_1 and f_2. It is a clear indication that the days on which EMIC wave occurrence is observed in the higher frequency range (>1 Hz) were preceded by higher magnetic activity. Such tendency was absent for the EMIC wave events associated with the lower frequency range (<1 Hz), which are dominantly seen in the afternoon–evening sector. The distribution of Kp_{max} and Dst_{min} showed in **Figures 7C,D** also supports a similar scenario. The peak in the distribution of $Kp_{\max}$ gradually shift from low values ≈4 for f_1 to high values ≈7 for $f_3 + f_4$. At the same time, the peak in the distribution of Dst_{min} gradually shift from high values ≈ − 30nT for f_1 to low values ≈ − 80nT for $f_3 + f_4$ frequency range. These tendencies suggest that mostly the higher frequency EMIC waves have occurred in the late recovery phase of a magnetic storm or after a few days following the geomagnetic disturbances.

4 DISCUSSION

In the present study, we have shown that the EMIC waves are mainly seen during the early morning, afternoon, and evening time sectors. The afternoon and evening time EMIC waves are attributed to magnetospheric compression due to solar wind pressure and nightside particle injection, respectively. Also, these afternoon–evening time EMIC waves are found to be associated with lower frequencies (<1 Hz), whereas, morning time EMIC waves have some link with the magnetic activity that occurred on preceding days, and mostly these waves have high frequencies (>1 Hz). The EMIC wave occurrence during the early morning, afternoon–evening sectors has been reported by

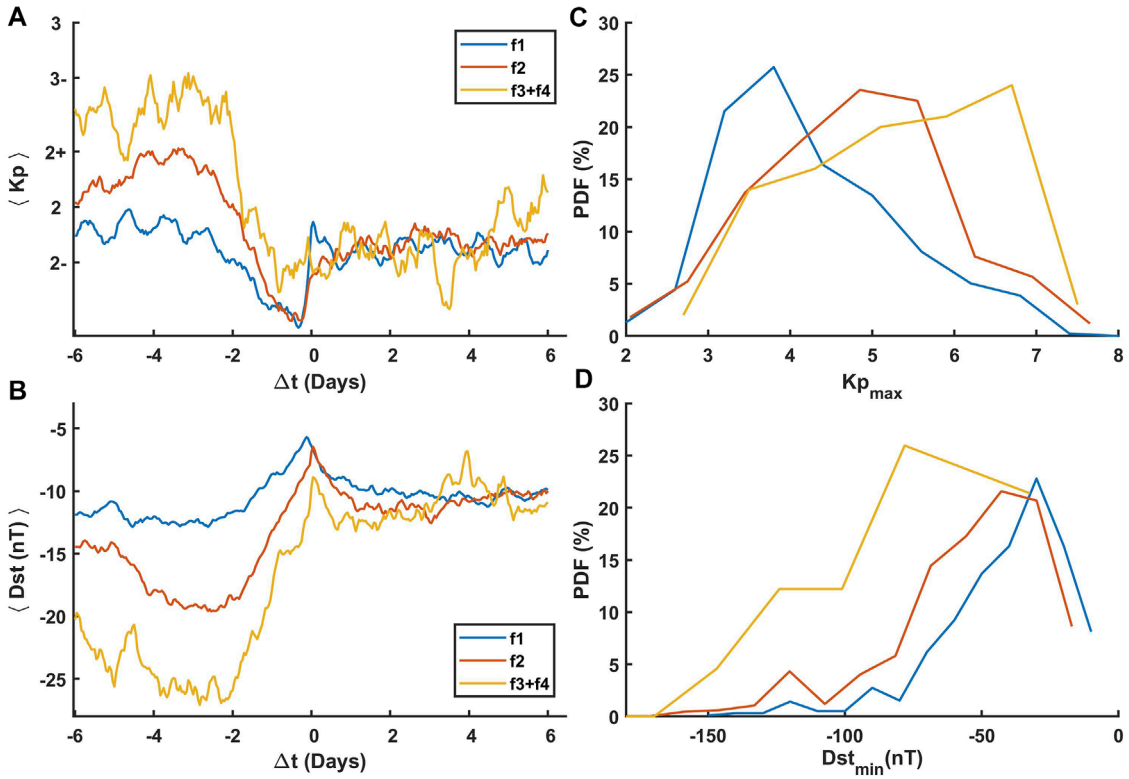

FIGURE 7 | Average values of **(A)** *Kp* and **(B)** *Dst* index for 6 days before and after the EMIC wave events are plotted as a function of $\Delta t = t - t_s$. Here, $\Delta t = 0$ indicates the start of the EMIC wave event. The probability distribution function of **(C)** maximum *Kp* and **(D)** minimum *Dst* occurring within 6 days prior to the occurrence of EMIC wave event are shown for f_1 (blue), f_2 (red), and $f_3 + f_4$ (yellow) frequency ranges.

various satellite observations of EMIC waves. These tendencies were attributed to two independent processes that cause the EMIC wave generation, that is, magnetospheric compression by the solar wind pressure and the energetic ion injections from the midnight sector (Keika et al., 2013; Kim et al., 2017; Remya et al., 2018). Min et al. (2012) also reported two peaks in the EMIC wave occurrence, one is in the dawn, which is dominated by the hydrogen band and another is in the dusk sector, which is dominated by the helium band. Although we are unable to relate the EMIC wave frequency observed on the ground to the gyro-frequency of the source ions (like *H+* or *He+*) responsible for the generation of these waves, the local time patterns observed on the ground are mere reflections of the local time occurrence of EMIC waves in space reported from the satellite observations.

Though we have some clue about the possible mechanism responsible for these preferred local times, however, one has to understand the difference in the frequencies for the early morning and afternoon–evening time EMIC waves. Using the AMPTE satellite Anderson et al. (1996), have observed diurnal patterns and reported differences in the characteristics of EMIC waves in the morning and afternoon time. These authors examined the generation conditions and found that actual ion temperature is low and the temperature anisotropy A_p ($=T_\perp/T_\parallel$) is higher during the morning hours in comparison with the afternoon. The relation of wave frequency to gyro frequency is given by $\Omega = \Omega_i[A_p/(A_p+1)]$. The value of $A_p/(A_p+1)$ was 0.37 for the noon event and 0.46 for the morning event. This difference in the temperature anisotropy could be a possible reason to see higher frequency waves during the morning. Moreover, during the afternoon–evening time, the cold plasma density is higher than that to dawn because of the presence of the plasmaspheric plume. High cold plasma density leads to a lower frequency of the waves during the afternoon–evening time (Horne and Thorne, 1994). There could also be a difference in the composition of the source ion population. Satellite studies (Van Allen probe) have also reported more H^+ band waves at dawn and He^+ band waves at dusk (Gamayunov et al., 2018).

5 SUMMARY AND CONCLUSION

In the present study, we have shown the diurnal distribution pattern of EMIC wave occurrence using seven years of ground observations from the Indian Antarctic station, Maitri. The EMIC waves were identified and their occurrence is noted in four different frequency ranges. Overall occurrence in different frequency ranges is summarized in **Table 1**. On the ground, we found two preferred local time sectors, namely, morning and afternoon–evening for the occurrence of EMIC waves. The

high-frequency (>1*Hz*) EMIC waves are mainly seen in the morning sector, whereas the low frequency (<1*Hz*) EMIC waves are prevalent in the afternoon–evening sector. These local time distributions of EMIC wave occurrence are examined in light of possible controlling parameters like solar wind dynamic pressure and *AE* index (a proxy for the substorm activity). The main outcomes of the present study are listed as follows:

1. The majority of the EMIC wave events observed at ground station Maitri are having a frequency below 1 Hz.
2. The total duration of EMIC wave occurrence in the seven years of the dataset is approximately 1969 h, 1083 h, 125 h, and 17 h in f_1 = 0.12–0.5 Hz, f_2 = 0.5–1 Hz, f_3 = 1–1.5 Hz, and f_4 = 1.5–2 Hz frequency ranges, respectively. We noticed that the EMIC wave occurrence on the ground decreases with an increase in the frequency range.
3. The diurnal distribution of EMIC wave occurrence clearly indicates that EMIC wave occurrence in the lower frequency range (<1 Hz) is prevalent between 13 and 23 LT hours, with a peak close to 15–18 h, whereas higher frequency (> 1 Hz) EMIC waves mainly occur in the early morning hours between 2 and 10 h, with a peak close to 6 LT hours.
4. On the ground, both solar wind pressure and *AE* index affect the overall diurnal distribution of EMIC waves in the lower frequency range (f < 1 Hz). The higher *AE* shifts the EMIC wave occurrence toward the dusk sector. It is attributed to fresh ion injections from the midnight sector during the substorm period, which is considered one of the possible triggering sources for the EMIC waves, whereas the afternoon time occurrence of the EMIC waves is found to be associated with the solar wind pressure, and it is in general agreement with earlier studies.
5. The morning time EMIC waves are less significantly affected by the level of *AE* index and solar wind pressure. In fact, these morning time high-frequency EMIC wave occurrences are associated with high magnetic activity on the proceeding days.

Recently, Chen et al. (2020) have investigated the role of *AE* and solar wind pressure separately using satellite observations and found that there exist two local time zones (i.e., afternoon 9–15 MLT and evening 16–20 MLT) for the generation of EMIC waves. The present study clearly indicates that the preferential local time zones reported by satellite for the EMIC wave occurrence are also evident in the ground observations. The study by Mann et al. (2014) has reported that although from the ground magnetometers the wave was 18+ hours long, the satellite coverage showed the wave lasted only for 10 – 15 min. Satellite observations are susceptible to bias based on their locations and coverage, which can be overcome by long-term ground observations. For a comprehensive picture of EMIC wave distribution and the particle dynamics in the Earth's magnetosphere, along with satellite studies, such a statistical study of EMIC wave observations using multi-ground stations will be useful, which is left as a future assignment.

DATA AVAILABILITY STATEMENT

The original contributions presented in the study are included in the article/Supplementary Material, further inquiries can be directed to the corresponding author.

AUTHOR CONTRIBUTIONS

The data analysis and original drafting of the manuscript were done by AU. BK helped in formulating the research problems and helped in interpretations. AK provided comments on the results and overall supervision. RR involved in technical support and data acquisition for ICM instruments.

ACKNOWLEDGMENTS

We thank OMNIWeb team for solar wind data available at http://omniweb.gsfc.nasa.gov and the WDC Kyoto for Dst, Ap, and Kp indices available at http://wdc.kugi.kyoto-u.ac.jp/. We thank the Polar team, IIG, for the ICM data.

REFERENCES

Allen, R. C., Zhang, J. C., Kistler, L. M., Spence, H. E., Lin, R. L., Klecker, B., et al. (2015). A Statistical Study of Emic Waves Observed by Cluster: 1. Wave Properties. *J. Geophys. Res. Space Phys.* 120, 5574–5592. doi:10.1002/2015ja021333

Anderson, B. J., Denton, R. E., Ho, G., Hamilton, D. C., Fuselier, S. A., and Strangeway, R. J. (1996). Observational Test of Local Proton Cyclotron Instability in the Earth's Magnetosphere. *J. Geophys. Res.* 101, 21527–21543. doi:10.1029/96ja01251

Anderson, B. J., Erlandson, R. E., and Zanetti, L. J. (1992). A Statistical Study of Pc 1-2 Magnetic Pulsations in the Equatorial Magnetosphere: 1. Equatorial Occurrence Distributions. *J. Geophys. Res.* 97, 3075–3088. doi:10.1029/91ja02706

Anderson, B. J., and Hamilton, D. C. (1993). Electromagnetic Ion Cyclotron Waves Stimulated by Modest Magnetospheric Compressions. *J. Geophys. Res.* 98, 11369–11382. doi:10.1029/93ja00605

Blum, L. W., Bonnell, J. W., Agapitov, O., Paulson, K., and Kletzing, C. (2017). Emic Wave Scale Size in the Inner Magnetosphere: Observations from the Dual Van allen Probes. *Geophys. Res. Lett.* 44, 1227–1233. doi:10.1002/2016gl072316

Bortnik, J., Cutler, J., Dunson, C., Bleier, T., and McPherron, R. (2008). Characteristics of Low-Latitude Pc1 Pulsations during Geomagnetic Storms. *J. Geophys. Res. Space Phys.* 113. doi:10.1029/2007ja012867

Cao, J. B., Ding, W. Z., Reme, H., Dandouras, I., Dunlop, M., Liu, Z. X., et al. (2011). The Statistical Studies of the Inner Boundary of Plasma Sheet. *Ann. Geophys.* 29, 289–298. doi:10.5194/angeo-29-289-2011

Chen, H., Gao, X., Lu, Q., Tsurutani, B. T., and Wang, S. (2020). Statistical Evidence for Emic Wave Excitation Driven by Substorm Injection and Enhanced Solar Wind Pressure in the Earth's Magnetosphere: Two Different Emic Wave Sources. *Geophys. Res. Lett.* 47, e2020GL090275. doi:10.1029/2020gl090275

Clausen, L., Baker, J., Ruohoniemi, J., and Singer, H. (2011). Emic Waves Observed at Geosynchronous Orbit during Solar Minimum: Statistics and Excitation. *J. Geophys. Res. Space Phys.* 116, 16823. doi:10.1029/2011ja016823

Cornwall, J. M. (1965). Cyclotron Instabilities and Electromagnetic Emission in the Ultra Low Frequency and Very Low Frequency Ranges. *J. Geophys. Res.* 70, 61–69. doi:10.1029/jz070i001p00061

Criswell, D. R. (1969). Pc 1 Micropulsation Activity and Magnetospheric Amplification of 0.2- to 5.0-Hz Hydromagnetic Waves. *J. Geophys. Res.* 74, 205–224. doi:10.1029/ja074i001p00205

Davis, T. N., and Sugiura, M. (1966). Auroral Electrojet Activity indexAEand its Universal Time Variations. *J. Geophys. Res.* 71, 785–801. doi:10.1029/jz071i003p00785

Engebretson, M. J., Posch, J. L., Wygant, J. R., Kletzing, C. A., Lessard, M. R., Huang, C. L., et al. (2015). Van allen Probes, Noaa, Goes, and Ground Observations of an Intense Emic Wave Event Extending over 12 H in Magnetic Local Time. *J. Geophys. Res. Space Phys.* 120, 5465–5488. doi:10.1002/2015ja021227

Erlandson, R. E., and Ukhorskiy, A. J. (2001). Observations of Electromagnetic Ion Cyclotron Waves during Geomagnetic Storms: Wave Occurrence and Pitch Angle Scattering. *J. Geophys. Res.* 106, 3883–3895. doi:10.1029/2000ja000083

Fu, H., Cao, J., Mozer, F., Lu, H., and Yang, B. (2012a). Chorus Intensification in Response to Interplanetary Shock. *J. Geophys. Res. Space Phys.* 117. doi:10.1029/2011ja016913

Fu, H. S., Cao, J. B., Zong, Q.-G., Lu, H. Y., Huang, S. Y., Wei, X. H., et al. (2012b). The Role of Electrons during Chorus Intensification: Energy Source and Energy Loss. *J. Atmos. solar-terrestrial Phys.* 80, 37–47. doi:10.1016/j.jastp.2012.03.004

Gamayunov, K. V., Min, K., Saikin, A. A., and Rassoul, H. (2018). Generation of Emic Waves Observed by Van allen Probes at Low L Shells. *J. Geophys. Res. Space Phys.* 123, 8533–8556. doi:10.1029/2018ja025629

Halford, A., Fraser, B., and Morley, S. (2010). Emic Wave Activity during Geomagnetic Storm and Nonstorm Periods: Crres Results. *J. Geophys. Res. Space Phys.* 115, 15716. doi:10.1029/2010ja015716

Horne, R. B., and Thorne, R. M. (1994). Convective Instabilities of Electromagnetic Ion Cyclotron Waves in the Outer Magnetosphere. *J. Geophys. Res.* 99, 17259–17273. doi:10.1029/94ja01259

Horne, R. B., and Thorne, R. M. (1997). Wave Heating of He+by Electromagnetic Ion Cyclotron Waves in the Magnetosphere: Heating Near the H+-He+bi-ion Resonance Frequency. *J. Geophys. Res.* 102, 11457–11471. doi:10.1029/97ja00749

Johnson, J. R., and Cheng, C. Z. (1999). Can Ion Cyclotron Waves Propagate to the Ground? *Geophys. Res. Lett.* 26, 671–674. doi:10.1029/1999gl900074

Jordanova, V. K., Farrugia, C. J., Thorne, R. M., Khazanov, G. V., Reeves, G. D., and Thomsen, M. F. (2001). Modeling Ring Current Proton Precipitation by Electromagnetic Ion Cyclotron Waves during the May 14-16, 1997, Storm. *J. Geophys. Res.* 106, 7–22. doi:10.1029/2000ja002008

Kakad, A., Kakad, B., Omura, Y., Sinha, A. K., Upadhyay, A., and Rawat, R. (2019). Modulation of Electromagnetic Ion Cyclotron Waves by Pc5 Ulf Waves and Energetic Ring Current Ions. *J. Geophys. Res. Space Phys.* 124, 1992–2009. doi:10.1029/2017ja024930

Keika, K., Takahashi, K., Ukhorskiy, A. Y., and Miyoshi, Y. (2013). Global Characteristics of Electromagnetic Ion Cyclotron Waves: Occurrence Rate and its Storm Dependence. *J. Geophys. Res. Space Phys.* 118, 4135–4150. doi:10.1002/jgra.50385

Kennel, C. F., and Petschek, H. E. (1966). Limit on Stably Trapped Particle Fluxes. *J. Geophys. Res.* 71, 1–28. doi:10.1029/jz071i001p00001

Kim, E. H., and Johnson, J. R. (2016). Full-wave Modeling of EMIC Waves Near the He + Gyrofrequency. *Geophys. Res. Lett.* 43, 13–21. doi:10.1002/2015gl066978

Kim, K. H., Omura, Y., Jin, H., and Hwang, J. (2017). A Case Study of Emic Waves Associated with Sudden Geosynchronous Magnetic Field Changes. *J. Geophys. Res. Space Phys.* 122, 3322–3341. doi:10.1002/2016ja023391

Liu, S., Xia, Z., Chen, L., Liu, Y., Liao, Z., and Zhu, H. (2019). Magnetospheric Multiscale Observation of Quasiperiodic Emic Waves Associated with Enhanced Solar Wind Pressure. *Geophys. Res. Lett.* 46, 7096–7104. doi:10.1029/2019gl083421

Mann, I. R., Usanova, M. E., Murphy, K., Robertson, M. T., Milling, D. K., Kale, A., et al. (2014). Spatial Localization and Ducting of Emic Waves: Van allen Probes and Ground-Based Observations. *Geophys. Res. Lett.* 41, 785–792. doi:10.1002/2013gl058581

McCollough, J., Elkington, S., Usanova, M., Mann, I., Baker, D., and Kale, Z. (2010). Physical Mechanisms of Compressional Emic Wave Growth. *J. Geophys. Res. Space Phys.* 115, 5393. doi:10.1029/2010ja015393

Meredith, N. P., Horne, R. B., Kersten, T., Fraser, B. J., and Grew, R. S. (2014). Global Morphology and Spectral Properties of Emic Waves Derived from Crres Observations. *J. Geophys. Res. Space Phys.* 119, 5328–5342. doi:10.1002/2014ja020064

Meredith, N. P., Thorne, R. M., Horne, R. B., Summers, D., Fraser, B. J., and Anderson, R. R. (2003). Statistical Analysis of Relativistic Electron Energies for Cyclotron Resonance with Emic Waves Observed on Crres. *J. Geophys. Res. Space Phys.* 108, 700. doi:10.1029/2002ja009700

Min, K., Lee, J., Keika, K., and Li, W. (2012). Global Distribution of Emic Waves Derived from Themis Observations. *J. Geophys. Res. Space Phys.* 117, 7515. doi:10.1029/2012ja017515

Morris, R. J., and Cole, K. D. (1991). High-latitude Day-Time Pc1-2 Continuous Magnetic Pulsations: A Ground Signature of the Polar Cusp and Cleft Projection. *Planet. Space Sci.* 39, 1473–1491. doi:10.1016/0032-0633(91)90076-m

Mursula, K., Anderson, B. J., Erlandson, R. E., and Pikkarainen, T. (1996). Solar Cycle Change of Pc1 Waves Observed by an Equatorial Satellite and on the Ground. *Adv. Space Res.* 17, 51–55. doi:10.1016/0273-1177(95)00694-a

Mursula, K., Kangas, J., Pikkarainen, T., and Kivinen, M. (1991). Pc 1 Micropulsations at a High-Latitude Station: A Study over Nearly Four Solar Cycles. *J. Geophys. Res.* 96, 17651–17661. doi:10.1029/91ja01374

Omura, Y., Pickett, J., Grison, B., Santolik, O., Dandouras, I., Engebretson, M., et al. (2010). Theory and Observation of Electromagnetic Ion Cyclotron Triggered Emissions in the Magnetosphere. *J. Geophys. Res.* 115, 15300. doi:10.1029/2010JA015300

Ozaki, M., Shiokawa, K., Horne, R. B., Engebretson, M. J., Lessard, M., Ogawa, Y., et al. (2021). Magnetic Conjugacy of Pc1 Waves and Isolated Proton Precipitation at Subauroral Latitudes: Importance of Ionosphere as Intensity Modulation Region. *Geophys. Res. Lett.* 48 (5) e2020GL091384. doi:10.1029/2020gl091384

Park, J. S., Kim, K. H., Shiokawa, K., Lee, D. H., Lee, E., Kwon, H. J., et al. (2016). EMIC Waves Observed at Geosynchronous Orbit under Quiet Geomagnetic Conditions (Kp ≤ 1). *J. Geophys. Res. Space Phys.* 121, 1377–1390. doi:10.1002/2015ja021968

Posch, J., Engebretson, M., Murphy, M., Denton, M., Lessard, M., and Horne, R. B. (2010). Probing the Relationship between Electromagnetic Ion Cyclotron Waves and Plasmaspheric Plumes Near Geosynchronous Orbit. *J. Geophys. Res. Space Phys.* 115, 446. doi:10.1029/2010ja015446

Regi, M., Marzocchetti, M., Francia, P., and De Lauretis, M. (2017). A Statistical Analysis of Pc1–2 Waves at a Near-Cusp Station in antarctica. *Earth, Planets and Space* 69, 1–16. doi:10.1186/s40623-017-0738-8

Remya, B., Sibeck, D. G., Halford, A. J., Murphy, K. R., Reeves, G. D., Singer, H. J., et al. (2018). Ion Injection Triggered EMIC Waves in the Earth's Magnetosphere. *J. Geophys. Res. Space Phys.* 123, 4921–4938. doi:10.1029/2018ja025354

Remya, B., Tsurutani, B. T., Reddy, R. V., Lakhina, G. S., and Hajra, R. (2015). Electromagnetic Cyclotron Waves in the Dayside Subsolar Outer Magnetosphere Generated by Enhanced Solar Wind Pressure: Emic Wave Coherency. *J. Geophys. Res. Space Phys.* 120, 7536–7551. doi:10.1002/2015ja021327

Sakaguchi, K., Shiokawa, K., Miyoshi, Y., and Connors, M. (2015). Isolated Proton Auroras and Pc1/EMIC Waves at Subauroral Latitudes. *Am. Geophys. Union (Agu))*, 59–70. doi:10.1002/9781118978719.ch5

Sandanger, M., Søraas, F., Aarsnes, K., Oksavik, K., and Evans, D. (2007). Loss of Relativistic Electrons: Evidence for Pitch Angle Scattering by Electromagnetic Ion Cyclotron Waves Excited by Unstable Ring Current Protons. *J. Geophys. Res. Space Phys.* 112, 138. doi:10.1029/2006ja012138

Summers, D., and Thorne, R. M. (2003). Relativistic Electron Pitch-Angle Scattering by Electromagnetic Ion Cyclotron Waves during Geomagnetic Storms. *J. Geophys. Res. Space Phys.* 108. doi:10.1029/2002ja009489

Thorne, R. M., and Kennel, C. F. (1971). Relativistic Electron Precipitation during Magnetic Storm Main Phase. *J. Geophys. Res.* 76, 4446–4453. doi:10.1029/ja076i019p04446

Upadhyay, A., Kakad, B., Kakad, A., Omura, Y., and Sinha, A. K. (2020). Occurrence Characteristics of Electromagnetic Ion Cyclotron Waves at Subauroral Antarctic Station Maitri during Solar Cycle 24. *Earth, Planets and Space* 72, 1–16. doi:10.1186/s40623-020-01157-7

Usanova, M. E., Darrouzet, F., Mann, I. R., and Bortnik, J. (2013). Statistical Analysis of Emic Waves in Plasmaspheric Plumes from Cluster Observations. *J. Geophys. Res. Space Phys.* 118, 4946–4951. doi:10.1002/jgra.50464

Usanova, M., Mann, I., Bortnik, J., Shao, L., and Angelopoulos, V. (2012). Themis Observations of Electromagnetic Ion Cyclotron Wave Occurrence: Dependence on Ae, Symh, and Solar Wind Dynamic Pressure. *J. Geophys. Res. Space Phys.* 117, 18049. doi:10.1029/2012ja018049

Usanova, M., Mann, I., Rae, I., Kale, Z., Angelopoulos, V., Bonnell, J., et al. (2008). Multipoint Observations of Magnetospheric Compression-Related Emic Pc1 Waves by Themis and Carisma. *Geophys. Res. Lett.* 35, 4458. doi:10.1029/2008gl034458

Wang, H., He, Y. F., Lühr, H., and Zhang, J. (2021). Local Time and Longitudinal Differences in the Occurrence Frequency of Ionospheric Emic Waves during Magnetic Storm Periods. *J. Geophys. Res. Space Phys.* 126, e2020JA028878. doi:10.1029/2020ja028878

Xue, Z., Yuan, Z., and Yu, X. (2021). Prompt Emergence and Disappearance of Emic Waves Driven by the Sequentially Enhanced Solar Wind Dynamic Pressure. *Geophys. Res. Lett.* 48, e2020GL091479. doi:10.1029/2020gl091479

Yu, X., Yuan, Z., Huang, S., Wang, D., Li, H., Qiao, Z., et al. (2017). Emic Waves Covering Wide L Shells: Mms and Van allen Probes Observations. *J. Geophys. Res. Space Phys.* 122, 7387–7395. doi:10.1002/2017ja023982

Yuan, Z., Xiong, Y., Huang, S., Deng, X., Pang, Y., Zhou, M., et al. (2014). Cold Electron Heating by Emic Waves in the Plasmaspheric Plume with Observations of the Cluster Satellite. *Geophys. Res. Lett.* 41, 1830–1837. doi:10.1002/2014gl059241

Conflict of Interest: The authors declare that the research was conducted in the absence of any commercial or financial relationships that could be construed as a potential conflict of interest.